Title

Systematic Evaluation of Self-Assembling Membrane Peptides to Form Nanopores in the context of the Functional Nanopore Screen

Authors

Klara Eisenhauer[1,2,§], Wadim Weber[1,2,§], Philipp Kemp[1,2] and Viktor Stein[1,2,*]

Affiliations

[1] Department of Biology, TU Darmstadt, 64287 Darmstadt, Germany;

[2] Centre for Synthetic Biology, TU Darmstadt, 64283 Darmstadt, Germany;

[§] These authors contributed equally

Corresponding Author

*Correspondence should be addressed to Viktor Stein, Tel. +49 6151 16 21947; Fax. +49 6151 16 22063; Email: stein@bio.tu-darmstadt.de

Abstract

The functional analysis of protein nanopores is typically conducted in planar lipid bilayers or liposomes exploiting high-resolution but low-throughput electrical and optical read-outs. Yet, the reconstitution of protein nanopores *in vitro* still constitutes an empiric and low-throughput process. Addressing these limitations, nanopores can now be analysed using the functional nanopore (FuN) screen exploiting genetically-encoded fluorescent protein sensors that resolve distinct nanopore-dependent Ca^{2+} in- and efflux patterns across the inner membrane of *Escherichia coli*. With a primary proof-of-concept established for the $S^{21}68$ holin, and thereof based recombinant nanopore assemblies, the question arises to what extent alternative nanopores can be analysed with the FuN screen. Focussing on self-assembling membrane peptides, three sets of 13 different nanopores are assessed for their capacity to form nanopores in the context of the FuN screen. Nanopores tested comprise both natural and computationally-designed nanopores while a comparison with high-resolution biophysical studies provides an experimental benchmark for future studies.

Key Words

FuN screen, nanopore, self-assembling membrane peptides, designer nanopore, holin

Main Manuscript

Protein nanopores comprise a versatile class of membrane proteins that are increasingly exploited across a range of biotechnological applications[1], most prominently DNA sequencing[2] and more recently proteins[3,4]. Further, nanopores can be modified with receptors turning them into exquisitely sensitive and specific molecular sensors[1]. A key bottleneck concerns our ability to study and engineer nanopores by experimental means which frequently relies on tailored expression and reconstitution protocols in lipid bilayers *in vitro*[5–7]. Addressing these limitations, the functional nanopore (FuN) screen exploits Ca^{2+}-responsive fluorescent protein (FP) sensors to resolve the functional properties of a nanopore according to distinct Ca^{2+} in- and efflux patterns across the *E. coli* inner membrane[8] (**Fig. 1A**).

Given its recent implementation and proof-of-concept with the $S^{21}68$ holin and thereof based recombinant assemblies, a question concerns to what extent alternative nanopores can be resolved with the FuN screen. Focussing on self-assembling membrane peptides, a representative set of nanopores was identified from the literature[9–12] and systematically evaluated using the FuN screen (**Tab. 1, Tab. S1**). Nanopores tested include a consensus design of the pore-forming module of the bacterial transmembrane protein Wza[9], a set of *de novo* designed nanopores featuring α-helical coiled-coil transmembrane (CCTM) structures[10], and the first transmembrane (TM1) domain of the Mϕ D29 holin[11,12].

In total, 11 out of 13 nanopores triggered characteristic Ca^{2+}-dependent signals as Ca^{2+}-permeable nanopores formed in the *E. coli* inner membrane (**Fig. 1B-E**). In general terms, the fluorescent signal along with the $T_{½}^{IPTG}$ turned out promoter dependent. In fact, for several nanopores – namely, $cWza^{Y373C}$, D29 $rTM1^{GP}$, D29 rTM1and to some extent D29 TM1 – expression from the stronger promoter turned out critical in generating a sigmoidally-shaped nanopore-dependent curve in the first place (**Fig. S1**, **Fig. S3**). Conversely, promoter strength did not impact the EDTA-dependent efflux rate, $T_{½}^{EDTA}$, as it provides a measure for the functional integrity of a nanopore independent of the underlying transcription, translation and assembly kinetics (**Tab. 1**). Further, a limited number of nanopores (e.g. cWza and $cWza^{Y373C}$) turned out toxic according to plateauing OD_{600}s but did not trigger a Ca^{2+}-dependent signal in the FuN screen (**Fig. 1B**, **Fig. S1**).

Further, a comparison with high-resolution biophysical studies recapitulates key trends underlying the functional properties of different nanopores tested: In case of a minimal Wza-derived transmembrane module[9] only a disulphide-stabilised mutant, $cWza^{K375C}$, but neither the primary consensus design, cWza, nor an alternative disulphide stabilised variant, $cWza^{Y373C}$, triggered a fluorescent signal in the FuN screen. These relative trends generally reflect the distribution of characteristic closed (C), low (L) and high (H) electrically conductive states (i.e. $cWza^{K375C}$ > cWza > $cWza^{Y373C}$)[9]. Alternatively, given cWza and $cWza^{Y373C}$ turn out

toxic as judged by plateauing OD_{600}s but did not trigger a Ca^{2+}-dependent signal, cWza and cWza^{Y373C} could exert specificity for Na^+ and K^+, but not Ca^{2+} with a larger hydration shell.
Further, a set of *de novo* designed, tetrameric α-helical CCTMs[10] triggered a rapid nanopore-dependent signal with distinct Ca^{2+} in- and efflux patterns (**Fig. 1C**, **Fig. S2**). Notably, CCTM-II yielded the highest absolute fluorescent signal along with the fastest $T_{½}^{IPTG}$ influx rates correlating with the most conductive states in electrochemical measurements[10]. In contrast, CCTM-LL and CCTM-VI displayed progressively lower absolute fluorescent signals and proportionately delayed $T_{½}^{IPTG}$ influx rates which is conclusive with lesser conductive states observed in electrochemical measurements[10]. Otherwise, EDTA-dependent efflux rates $T_{½}^{EDTA}$ proved highly similar for different CCTM variants suggesting that, at least in the context of the FuN screen, CCTM variants primarily differ in their propensity to assemble into Ca^{2+}-permeable nanopores. In addition, a hybrid nanopore featuring one LL and two VI motifs at critical α-helix packing sites yielded intermediate Ca^{2+}-dependent in- and efflux rates highlighting substantial plasticity in the underlying CCTM scaffold.
Finally, the FuN screen could recapitulate key features underlying the formation of nanopores by the D29 TM1 holin[11,12]. Previous studies showed that D29 TM1 undergoes a structural transition from β-hairpin to α-helix first triggering local membrane depolarisation before facilitating further insertion and assembly of D29 TM1 nanopores to result in complete permeabilisation[11,12]. Strikingly, sequence-permutated variants are limited to α-helical conformations and form defined ion channels[11,12]. Notably, the FuN screen recapitulates many of these features as variants with a strong β-hairpin propensity – namely, TM1, tTM1 and trTM1[26] – triggered an early increase in the Ca^{2+}-dependent signal as judged by a $T_{½}^{IPTG}$ (**Fig. 1D**, **Fig. S3**). In contrast, D29 TM1 variants that are restricted to a α-helical conformation – namely, rTM1 and rTM1^{GP} – need to accumulate to a higher concentration before triggering a late, but strong increase in the fluorescent signal (**Fig. 1E**, **Fig. S3**). Conversely, EDTA-dependent $T_{½}^{EDTA}$ efflux rates were reduced approximately 2-fold for TM1, tTM1 and trTM1[26] relative to rTM1 and rTM1^{GP} (**Tab. 1**). This could for once be due to fewer nanopores being synthesised before the inner membrane is permeabilized and adversely impacts their expression. Alternatively, this may arise from the formation of more transient and thus less Ca^{2+} permeable nanopores as has been implicated in prior electrochemical measurements[12]. Only sTM1 proves an exception as it forms nanopores early while displaying slower EDTA-dependent efflux rates despite a strong α-helical propensity in lipid micelles and ion channel-like properties in electrochemical measurements[12]. In this regard, one should note that a two-phase exponential decay provides a better fit for EDTA-dependent efflux rates compared to a one-phase model (**Fig. S4**). In fact, in this case, the faster EDTA-dependent efflux rate approximates the efflux rate observed for rTM1 and rTM1^{GP} which potentially implicates two distinct populations of high and low conductive sTM1.

To conclude, systematically evaluating the pore-forming propensity of 13 different self-assembling membrane peptides underpins the FuN screen as a complementary approach to high-resolution biophysical studies in reconstituted lipid bilayers. While it lacks the sensitivity and specificity of electrochemical measurements[5], it combines the scalability and ease of cellular assays with throughput and kinetic resolution. In a limited number of cases, discrepancies with biophysical studies in general and electrochemical measurements in particular arise but several factors need to be born in mind: Firstly, electrical conductivity is typically resolved using Na^+ and K^+ ions while the FuN screen exploits Ca^{2+} with a larger hydration shell which may for instance account for differences observed in the permeability of cWza variants. Secondly, *in vitro* bilayer measurements are conducted under highly controlled membrane potentials while in the FuN screen, owing to intracellular expression, the membrane potential is initially negative before turning neutral upon permeabilization. Finally, membrane composition in *E. coli* and reconstituted lipid bilayers differs. The latter is highly defined, yet potentially contains residual organic solvents and may also feature non-natural lipids such as DPhPC which may impact the functional properties of any given nanopore or ion channel.

Supporting Information

Supporting Information includes **(i)** a detailed account of the materials and methods and **(ii)** fluorescent recordings of all self-assembling membrane peptides.

Acknowledgements

The authors acknowledge support by Felix Herrmann assisting with experimental efforts.

Funding

LOEWE iNAPO, Hessen State Ministry of Higher Education, Research and the Arts (VS); Pioneer ACTIVATOR (Project No. 527 00 962), TU Darmstadt (VS).

References

(1) Wang, S.; Zhao, Z.; Haque, F.; Guo, P. Engineering of Protein Nanopores for Sequencing, Chemical or Protein Sensing and Disease Diagnosis. *Current Opinion in Biotechnology*. 2018.

(2) Wang, Y.; Yang, Q.; Wang, Z. The Evolution of Nanopore Sequencing. *Front. Genet.* **2014**, *5* (DEC).

(3) Brinkerhoff, H.; Kang, A. S. W.; Liu, J.; Aksimentiev, A.; Dekker, C. Multiple Rereads of Single Proteins at Single-Amino Acid Resolution Using Nanopores. *Science (80-.).* **2021**, *374* (6574).

(4) Zhang, S.; Huang, G.; Versloot, R. C. A.; Bruininks, B. M. H.; de Souza, P. C. T.;

Marrink, S. J.; Maglia, G. Bottom-up Fabrication of a Proteasome–Nanopore That Unravels and Processes Single Proteins. *Nat. Chem.* **2021**, *13* (12).

(5) Gutsmann, T.; Heimburg, T.; Keyser, U.; Mahendran, K. R.; Winterhalter, M. Protein Reconstitution into Freestanding Planar Lipid Membranes for Electrophysiological Characterization. *Nat. Protoc.* **2015**, *10* (1), 188–198.

(6) Fujii, S.; Matsuura, T.; Sunami, T.; Kazuta, Y.; Yomo, T. In Vitro Evolution of α-Hemolysin Using a Liposome Display. *Proc. Natl. Acad. Sci. U. S. A.* **2013**, *110* (42), 16796–16801.

(7) Heron, A. J.; Thompson, J. R.; Cronin, B.; Bayley, H.; Wallace, M. I. Simultaneous Measurement of Ionic Current and Fluorescence from Single Protein Pores. *J. Am. Chem. Soc.* **2009**, *131* (5), 1652–1653.

(8) Weber, W.; Roeder, M.; Probanowski, T.; Yang, J.; Abujubara, H.; Koeppl, H.; Tietze, A.; Stein, V. Functional Nanopore Screen: A Versatile High-Throughput Assay to Study and Engineer Protein Nanopores in Escherichia Coli. *ACS Synth. Biol.* **2022**.

(9) Mahendran, K. R.; Niitsu, A.; Kong, L.; Thomson, A. R.; Sessions, R. B.; Woolfson, D. N.; Bayley, H. A Monodisperse Transmembrane α-Helical Peptide Barrel. *Nat. Chem.* **2017**, *9*, 411–419.

(10) Scott, A. J.; Niitsu, A.; Kratochvil, H. T.; Lang, E. J. M.; Sengel, J. T.; Dawson, W. M.; Mahendran, K. R.; Mravic, M.; Thomson, A. R.; Brady, R. L.; et al. Constructing Ion Channels from Water-Soluble α-Helical Barrels. *Nat. Chem.* **2021**, *13*, 643–650.

(11) Lella, M.; Kamilla, S.; Jain, V.; Mahalakshmi, R. Molecular Mechanism of Holin Transmembrane Domain i in Pore Formation and Bacterial Cell Death. *ACS Chem. Biol.* **2016**, *11* (4), 910–920.

(12) Lella, M.; Mahalakshmi, R. Engineering a Transmembrane Nanopore Ion Channel from a Membrane Breaker Peptide. *J. Phys. Chem. Lett.* **2016**, *7*, 2298–2303.

Figures and Figure Captions

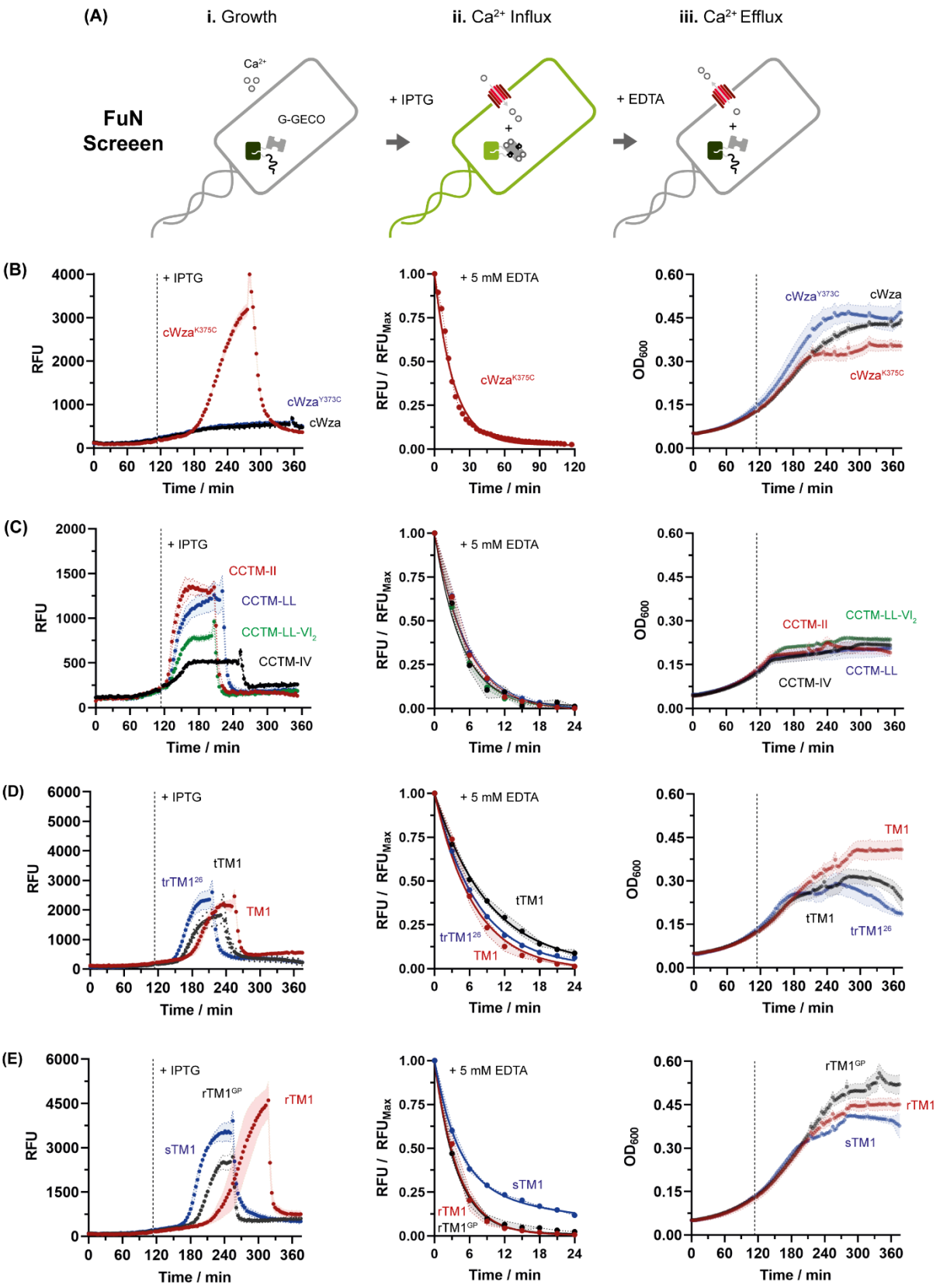

Figure 1: Schematic overview of the FuN screen: **(A)** Ca^{2+}-specific FP sensors resolve the functional properties of protein nanopores according to distinct Ca^{2+} in- and effluxes patterns across the inner membrane of *E. coli*; **(B-E)** Summary of kinetic traces used to characterise the functional properties of 13 different nanopores based on the $T_{½}^{IPTG}$ and $T_{½}^{EDTA}$. The EDTA-dependent decay is shown in a normalised fashion to facilitate comparisons. Nanopores tested include **(B)** a consensus design stabilised transmembrane module of cWza, **(C)** a set of computationally-designed nanopores based on α-helical coiled-coil transmembrane (CCTM) motifs, and **(D, E)** a set of nanopores that have been derived from the first transmembrane (TM1) domain of the Mϕ D29 holin. Nanopores were expressed in the context of the pCtrl2 from the stronger promoter (T7.100.WT) using 0.5 mM IPTG before the fluorescent signal was quenched with 5 mM EDTA. An averaged, time-dependent signal based on three independently picked colonies is shown.

Table 1: Systematic evaluation of 13 self-assembling membrane peptides in the context of the FuN screen at two different promoter strengths using Ca^{2+}-responsive FP sensors.

Nanopore	T7.100.sRBS		T7.100.wt.sRBS		Key Features According to Original Publication
	$T_{½}^{IPTG}$	$T_{½}^{EDTA}$	$T_{½}^{IPTG}$	$T_{½}^{EDTA}$	
cWza	-	-	-	-	Defined P-, L- and H-states[9]
$cWza^{Y373C}$	-	-	-	-	Less stabilised H-state[9]
$cWza^{K375C}$	-	-	107.5 ± 0.5	11.3 ± 0.1	More stabilised H-state[9]
CCTM-II	28.2 ± 0.6	3.0 ± 0.1	19.9 ± 0.9	3.8 ± 0.2	Large Conductivity[10]
CCTM-LL	39.8 ± 0.6	3.3 ± 0.1	25.0 ± 1.8	3.9 ± 0.2	Gating | Monodisperse[10]
CCTM-VI	41.9 ± 5.3	2.9 ± 0.2	33.2 ± 0.6	3.2 ± 0.2	Stable | Monodisperse[10]
CCTM-LL-VI_2	37.9 ± 0.7	3.5 ± 0.1	27.4 ± 0.6	3.2 ± 0.1	New Recombinant
D29 trTM[26]	84.4 ± 0.7	5.3 ± 0.1	53.2 ± 0.7	5.0 ± 0.1	Membrane Breaker[11]
D29 tTM1	129.7 ± 1.0	5.9 ± 0.1	63.5 ± 1.0	6.3 ± 0.2	Membrane Breaker[11]
D29 sTM1	138.2 ± 0.6	6.7 ± 0.2[$]	79.6 ± 1.9	5.0 ± 0.2[§]	Ion Channel[11]
D29 TM1	-	-	83.6 ± 3.1	4.7 ± 0.3	Membrane Breaker[11]
D29 rTM1	-	-	93.4 ± 0.5	2.8 ± 0.2	Ion Channel[11]
$D29\ rTM1^{GP}$	-	-	147.4 ± 2.9	2.7 ± 0.2	Ion Channel[11]

[§] Alternatively, a two-phase model yields: $T_{½}^{EDTA}$ (Fast): 2.8 ± 0.1; $T_{½}^{EDTA}$ (Slow): 20.6 ± 0.9; %-Fast: 0.72 ± 1.1

[$] Alternatively, a two-phase model yields: $T_{½}^{EDTA}$ (Fast): 3.0 ± 0.2; $T_{½}^{EDTA}$ (Slow): 18.3 ± 0.9; %-Fast: 0.59 ± 3.6